Magazine of Civil Engineering

ISSN 2712-8172

journal homepage: http://engstroy.spbstu.ru/

DOI: 10.34910/MCE.106.12

Impact of elevated temperature on the behavior of strengthened RC beams with CFRP

R. Al-Rousan

Jordan University of Science and Technology, Irbid, Jordan

E-mail: rzalrousan@just.edu.jo

Keywords: reinforced concrete, elevated temperature, flexural strength, fiber reinforced polymer, experimental

Abstract. Elevated temperatures (beyond 500°C) severely deteriorate concrete structures due to vapor pressure, decomposition of cement hydration products, inhomogeneous volume changes of concrete's ingredients. Carbon fiber-reinforced polymer (CFRP) composite materials provide the most significant retrieval of the structural performance to severely heat-damaged structural concrete members. Therefore, an experimental study investigated the influence of elevated temperatures on the flexural behavior of reinforced concrete (RC) beams strengthened externally with CFRP. For this purpose, thirty-two reinforced concrete beams were cast. Twenty-four beams were externally strengthened with CFRP, and eight beams were unanchored and left as a control. The beams then were tested under four-point bending to assess their structural performance in terms of failure modes and load-displacement relations. The experimental results have clearly shown that the control beams suffered from ductile failure. The CFRP strengthened beams failed by debonding the CFRP sheets after yielding the flexural steel reinforcement. The strengthened beams showed an increase in the ultimate load-carrying capacity accompanied by an enhancement in mid-span deflection in different percentages concerning the control beam. The CFRP sheets' ability in the bridging of the crack increased with the increase of CFRP length by providing more development length in catching the two sides of the major flexural crack. The load-deflection curve can be divided into two stages; the first portion is nearly a straight line, and the second stage with slope experienced a slight increase in the load with a large increase in deflection. The second stage formed after the yielding of steel reinforcement and formation of the main flexural crack where the applied load was carried by the CFRP sheet. Finally, the influence of the exposure temperature on the ductility, energy absorption, and ultimate load reduction percentage increases with the increase of temperature.

1. Introduction

Nowadays, the primary rehabilitation and strengthening composite materials of flexure or shear deficient reinforced concrete (RC) structures are carbon-fiber-reinforced polymer materials (CFRP). The CFRP external strengthening of the concrete structure increased the shear or flexural capacity. This composite material's integrity depends on the bond condition and how it can transfer stress from the concrete debonding surface to CFRP composite materials. The reliability of the bond between the concrete surface to CFRP composite materials determines the accomplishment of externally strengthening of deficient RC members. The significant considerations consist of CFRP composite material type, the number of CFRP composite, surface preparation, bonded length, laminate, and epoxy quality application.

CFRP materials are frequently used in structural engineering applications for the repair and strengthening of existing concrete structures. Externally bonded FRP composite is used to strengthen concrete beams in flexure and shear. Many experimental observations indicated that the debonding at the interface between concrete and FRP is a typical failure mode of reinforced concrete beams strengthened with externally bonded CFRP [1, 2]. CFRP composite materials have come to the forefront as promising

Al-Rousan, R. Impact of elevated temperature on the behavior of strengthened RC beams with CFRP. Magazine of Civil Engineering. 2021. 106(6). Article No. 10612. DOI: 10.34910/MCE.106.12

materials and systems for structural retrofit. Glass fiber reinforced polymer (GFRP) and carbon fiber reinforced polymer (CFRP) have higher tensile strength but its strength is not fully utilized due to debonding problem and brittle tensile behavior. The general influence is clearly an increase in the peak loads of the specimens [3, 4].

Elevated temperatures cause severe damage for reinforced concrete (RC) structures, such as RC beams. RC beams have been reported to loss strength and stiffness with relatively large permanent deformations because of exposure to high temperatures [5]. These harmful effects could be attributed to the deterioration of mechanical characteristics of concrete and steel rebars and the redistribution of stresses within the beam due to the elevated temperatures [5, 6]. Currently, the most commonly used technique to repair the heat-damaged RC beams is using CFRP composites. These sheets are advanced materials that can be easily applied to the structures and characterized by outstanding mechanical and corrosion resistance characteristics. Various studies were performed to investigate the flexural behavior of RC beams wrapped with CFRP. The results showed that externally bonded CFRP sheets and laminates enhance the beams' flexural behavior and recover, to a specific limit, the flexural strength of heat-damaged beams. Strengthening level of recovery depends on several factors such as fire resistance [7], elevated temperature [8, 9], fiber type [10–13], analysis type [14–18], energy integrity resistance [19], anchored system [20], heating condition [21, 22], degree of beam's damage and geometry and type of fiber sheet [23], and safety factors for CFRP strengthening of bridges [24].

Reinforcing concrete structures are often subjected to heating cycles–cooling such as in chimneys, concrete foundations for launching rockets carrying spaceships, concrete near to the furnace, clinker silos, and nuclear power plants, or those subjected to fire then extinguished using water. Temperature cycles are critical to the stability of concrete structures and require considerations upon design [25, 26]. As well stipulated, the mechanical properties of concrete are preserved for exposure temperatures below 300 °C, yet are decreased considerably as the temperature exceeds 500 °C [27]. Additional damage results from rabid cooling such as in the case of distinguishing of fire with cool water due to creation of temperature gradient between concrete core and its surface. This results in tensile stresses on the concrete surface that are high enough to crack concrete, and this is considered as another source of damage results from incompatible expansion and contraction of aggregate and surrounding cement paste. The magnitude of damage is influenced by many factors such as the size of concrete members, the type of cement and aggregate, the concrete moisture content, and the predominant environmental factors, those are represented in heating exposure time, and rate, type of cooling, and maximum temperature attained [28]. Different types of materials and techniques were used in strengthening and retrofitting existing concrete structures, such as steel plate bolting, reinforced concrete jackets, prestressed external tendons, and most recently, CFRP composite which has been used on a large scale in different countries. CFRP composites have many advantages over conventional methods represented in ease of application, high strength-to-weight ratio, excellent mechanical strength, and good resistance to corrosion, especially that most structures are damaged due to dynamic loads, corrosion of steel, and freeze-thaw cycles as well as the CFRP composites have disadvantages such as the low ductility of CFRP compared to steel, low fire resistance, problematic bonding to the structure [29–31].

This research will be useful for retrofitting the existing buildings, mainly for buildings exposed to elevated temperatures. Furthermore, the ACI 440 guideline [30] concluded that the behavior and endurance of FRP-reinforced concrete structures under exposure to high heat is still not well understood. Therefore, essential issues to produce effective, economical, and successful CFRP strengthening were needed. Also, the impact of CFRP external strengthening on the behavior of flexural deficient reinforced concrete beams exposed to elevated temperature must receive miniature consideration. The scientific problem considered in the study is indeed one of the problems in the modern theory of flexural deficient reinforced concrete beams. A lack of literature regarding flexural behavior of deficient beams exposed to elevated temperature necessitated conducting the present investigation. In this study, experimental program was carried out to find the improvements in the strength and ductility behavior of RC beams confined externally with CFRP. The main parameters studied were the length of CFRP sheets (400, 600, and 800 mm) and elevated temperature (23 °C, 150 °C, 250 °C, and 500 °C).

2. Methods

2.1. Experimental Work

Thirty-two (two beams were made from each type) beams were casted and tested as simply supported under four points' loading, as shown in Fig. 1. The tested beams were 1100 mm long with cross-sectional dimensions of 150×250 mm. The investigated parameters in this study are the length of CFRP sheets (400, 600, and 800 mm) and elevated temperature (23 °C, 150 °C, 250 °C, and 500 °C) as shown in Table 1. The designation and steel reinforcement (yielding stress of 420 MPa) of the tested beams are summarized in Table 1 and Fig. 1, respectively.

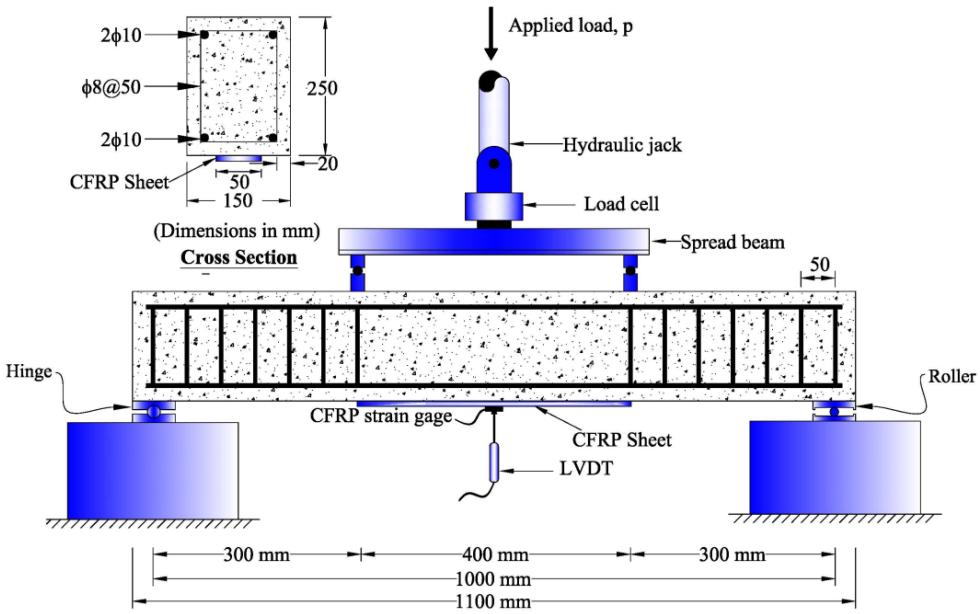

Figure 1. Setup and reinforcement details of the beams.

Table 1. The details of failure of tested shear beams.

Group	Specimen	T, °C	CFRP Configuration	P_u, kN	Δ_u, mm	ε_f, με	$\varepsilon_f / \varepsilon_{fu}$,%
1	FBT23-0	23	None	101.1	10.8	---	---
	FBT23-400		CFRP sheet (length of 400 mm and width of 50 mm)	113.8	12.5	4685	0.28
	FBT23-600		CFRP sheet (length of 600 mm and width of 50 mm)	121.7	14.0	5750	0.34
	FBT23-800		CFRP sheet (length of 800 mm and width of 50 mm)	132.2	15.8	6858	0.41
2	FBT150-0	150	None	95.3	10.5	---	---
	FBT150-400		CFRP sheet (length of 400 mm and width of 50 mm)	108.7	11.6	4279	0.26
	FBT150-600		CFRP sheet (length of 600 mm and width of 50 mm)	117.4	12.1	5285	0.32
	FBT150-800		CFRP sheet (length of 800 mm and width of 50 mm)	128.8	13.2	6326	0.38
3	FBT250-0	250	None	82.7	9.9	---	---
	FBT250-400		CFRP sheet (length of 400 mm and width of 50 mm)	95.5	10.7	3817	0.23
	FBT250-600		CFRP sheet (length of 600 mm and width of 50 mm)	103.1	11.2	4323	0.26
	FBT250-800		CFRP sheet (length of 800 mm and width of 50 mm)	113.1	12.1	5163	0.31
4	FBT500-0	500	None	62.7	9.3	---	---
	FBT500-400		CFRP sheet (length of 400 mm and width of 50 mm)	72.6	9.9	3334	0.20
	FBT500-600		CFRP sheet (length of 600 mm and width of 50 mm)	79.6	10.4	3890	0.23
	FBT500-800		CFRP sheet (length of 800 mm and width of 50 mm)	87.3	10.6	4343	0.26

Note: The values between parentheses are normalized with respect to the control, T: Temperature, P_u : Ultimate Load, Δ_u : Ultimate deflection, ε_f = CFRP strain, ε_{CFRP} is the strain in CFRP strips and ε_{fu} is the ultimate strain in CFRP strips of 16700 με.

2.2. Mix design

Table 2 shows the design of concrete mixture with the proportions by weight of water to cement ratio (w/c) of 0.59:1.00(cement (Ordinary Type I Portland cement)):2.98(Crushed limestone coarse aggregates

with the absorption of 2.3 %, a maximum aggregate size of 12.5 mm, and a specific gravity of 2.62)):2.62 (fine aggregates with the absorption of 1.9 %, fineness modulus of 2.69, and specific gravity of 2.65). The superplasticizer as a percent of the cement weight was used to improve the concrete mixture's workability and result in a slump of about 50 mm.

Table 2. Mix design proportions.

Ingredient	Quantity (kg/m³)
Cement	269
Water	158
w/c	0.59
Super- plasticizer	8
Coarse aggregate	891
Fine aggregate	834

The beams are casted using a tilting drum mixer with a capacity of 0.15 m³ (Fig. 2). Firstly, the tilting drum mixer inner surface was wetted. During the tilting drum mixer running, all the crushed limestone coarse aggregates with portion of the used water were added (Fig. 2). After that, the fine aggregates, cement, and water were added gradually. Finally, the superplasticizer with the last amount of used water was added to the concrete mixture. Lastly, all the concrete mixture ingredients were mixed for five minutes before pouring into wooden molds with inner dimensions of (100×150×1100 mm) and compacted with an electrical vibrator (Fig. 2). After twenty-four hours from the beams casting, all beams were de-molded and then cured in lime-saturated water tank for 28 days (Fig. 2).

Preparing the ingredients of mixture

Mixing concrete by tilting drum mixer

Wooden mold for casting beams

Casting concrete into molds

Casting concrete into cylinders

Water-cured tank for 28 days

Figure 2. The mixing, casting, and curing of reinforced concrete beams.

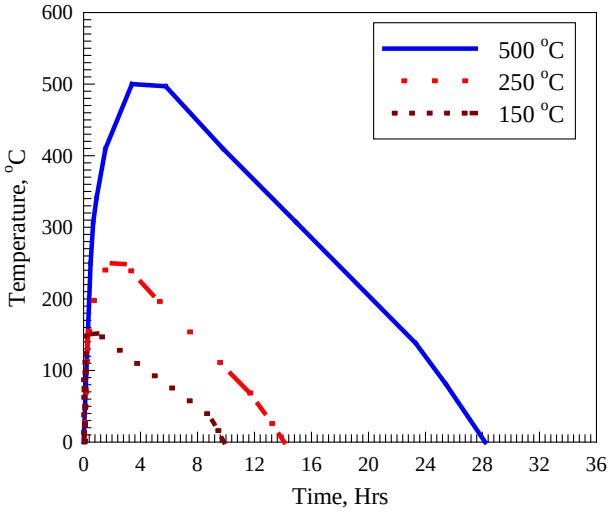

Figure 3. The time-temperature schedule.

2.3. Heat treatment Method

The average 28-day splitting compressive and tensile strengths of the tested cylinders were 25.0 MPa and 3.0 MPa, respectively. Cylindrical specimens and blocks were subjected to heat treatment for two hours at temperatures from 150-500 °C before allowing them to cool inside the special electrical furnace. The furnace is equipped with an electronic panel to automatically control the time of exposure and the temperature (maximum of 1200 °C). Fig. 3 shows the time-temperature schedule for the furnace. The expected temperature inside the beam during the heat treatment method is 28 % of the applied temperature on the exposed surface [30].

The effect of exposing specimens to elevated temperatures is demonstrated in Fig. 4, which depicts the residuals for compressive and slitting strength versus temperature. The curves followed almost similar trend behavior represented in a slight decrease at a temperature of 150 °C followed by a significant reduction at higher temperatures. The detrimental effect of high temperatures greater than 250 °C on both strengths can be referred to as thermally induced cracks and/or decomposition of cement binding materials (beyond 250 °C) [27]. The damage by heating caused map type cracking, which increased with elevated temperature without being accompanied by an apparent surface alteration. The reduction in residual strengths (compressive, splitting) which is (98 %, 97 %) at 150 °C to (61 %, 60 %) at 500 °C, are similar to reported values by Haddad et al. [27] as can be deduced from Fig. 4.

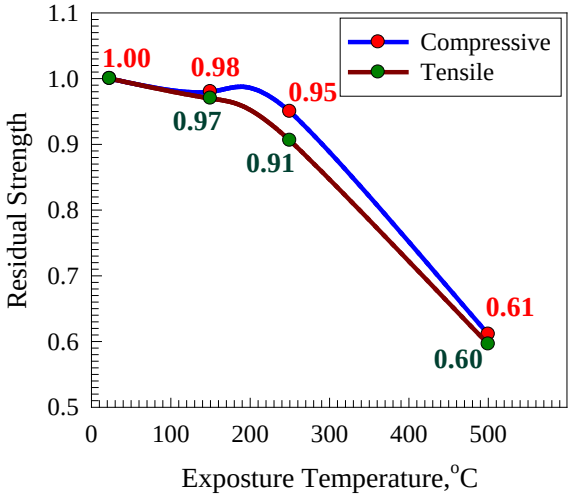

Figure 4. Residuals for compressive and splitting strengths versus exposure temperature.

2.4. Bonding of CFRP sheets to the concrete beams

The concrete beams were demolded after 24 hours of casting and cured in a lime-saturated water tank for 28 days. Firstly, the concrete bonded area was roughened and brushed with steel wire cup brush to provide leveled contact between CFRP sheets and concrete (Fig. 5). Secondly, any dust and loose particles were removed from the bonded area by using the air vacuum cleaner, and then the bonded area

was marked while the un-bonded area was covered with plastering tape to be free of epoxy (Fig. 5). Based on investigated parameters, the CFRP composite sheets are cut into sheets with a width of 50 mm and different lengths. Thirdly, the epoxy compounds (parts A and B) were prepared using a low-speed electric drill for at least 3 minutes to get a homogenous epoxy mixture. Fourthly, the epoxy first layer was applied uniformly over the bonded area and then the CFRP composite sheet (the tensile strength of 4900 MPa, thickness of 0.166 mm, elongation at break of 2.1 %, elastic modulus of 230 GPa) was placed onto the epoxy. Plastic roller was used along the fiber direction in order to remove any entrapped air bubbles. Finally, the epoxy second layer was applied over the CFRP sheet bonded area to make sure epoxy homogeneous distribution (Fig. 5).

Marking the area of CFRP sheets bonded using plastering tape

Concrete bonded area were roughened and brushed with steel wire cup brush

Applying the first layer of epoxy onto CFRP sheets surface

Applying the two layers of epoxy onto CFRP sheets surface

Figure 5. Bonding of CFRP sheets to reinforced concrete beams.

2.5. Testing Setup

All beams were tested under four-point loading with a simply supported span of 1000 mm (Fig. 1). The two supports are one roller, and the other one is a hinge, as well as the loading points were made from steel to make sure zero deformation. A hydraulic testing machine is used to apply the load with a displacement loading rate of 0.1 mm/sec. The vertical linear variable displacement transducer (LVDT) is used to record the mid-span deflection which is placed at the bottom of the beam (Fig. 1). Also, one strain gauge was placed in a position such that to record the CFRP tensile strain. The tested results (load-deflection curves and the CFRP strain) were collected using the data acquisition system, while the failure modes and cracks pattern were obtained visually.

3. Results and Discussion

3.1. Failure Mode

The crack patterns and mode of failure developed during testing of all RC beams are shown in Fig. 6. In control beam, the first crack appeared in the middle of the constant moment region followed by formation of additional nearby flexural cracks (Fig. 6(a)). In all beams, the first flexural crack developed in the middle of the beam and at the tension side (within the constant moment region) (Fig. 6(b)).

23 °C

250 °C

150 °C

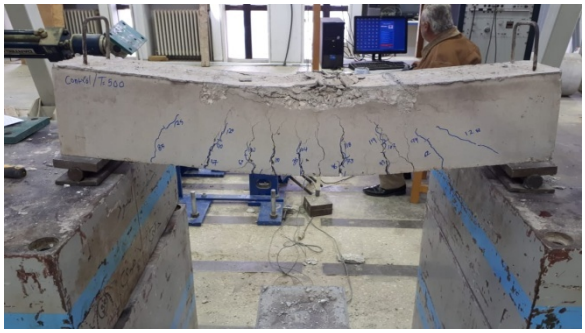

500 °C

(a) Effect of elevated temperature

0 mm (Control)

400 mm

600 mm

800 mm

(b) Effect of CFRP bonded length

Figure 6. The typical failure mode of tested beams.

The failure in the control beams (conventionally reinforced) occurred by yielding steel reinforcement followed by the crushing of the concrete in the beams' compression zone in the constant moment region. As load approached failure, local concrete crushing under the loading points was observed, as shown in Fig. 6(a). The strengthened beams failed by debonding the CFRP sheets after yielding the flexural steel reinforcement except the ductile flexure failure shown in Fig. 6(b). Upon yielding the steel reinforcement, the CFRP sheet picked up more strains and contributed to the beams' further load carrying capacity. After

failure, the CFRP sheet partially delaminated and it was observed that the sheet had adhered well to the concrete. The additional strength provided by the CFRP sheet delayed cracking and increased the load carrying capacity of the beams after yielding of steel occurred. It was noticed that the cracks numbers, distribution and length visibly depends on the CFRP sheet length (Fig. 6(b)). Inspection Fig. 6 reveals that crack distribution and numbers increased with the increase of elevated temperature (Fig. 6(a)) and length CFRP sheet length (Fig. 6(b)). As a matter of fact, Ahmed et al. [32] reported all the beams failed by flexural failure mode and the tested beams reveal a dramatic effect and spalling in the concrete cover, especially at temperature of 500 °C and more as well as at the end of the testing some crushing cracks caused by compression failure appeared at the top surface. But the crack from the tension side up to top of the cracking section neutral axis decreased with the increase of the elevated temperature (Fig. 6(a)) and length CFRP sheet length (Fig. 6(b)). The increase in crack width and the reduction in beam capacity after the elevated temperature is due to the residual concrete strength after elevated temperature exposure, which is much lower than that at room temperature [32]. This is due to the CFRP sheets ability in the bridging of the flexural cracks by providing adequate development length in catching the two sides of the major flexural crack.

3.2. CFRP strain

Fig. 7 shows the typical load-CFRP strain curve for all tested beams. Fig. 7 reveals that the tensile stresses develop in the CFRP composites after the yielding of the steel reinforcement. Furthermore, the maximum tensile stresses occurred close to the middle of the CFRP composite that intersects the first flexural crack to the beam's mid-span, as shown in Fig. 7. Also, it is noticed that all tested beams had CFRP strain below the maximum value of 16700 με as shown in Table 1 as the percentage of CFRP ultimate strain. Inspection of Table 1 reveals that the length of CFRP sheets had a substantial immct on the efficiency of CFRP sheets for beams exposed to 23ºC with a percentage concerning ultimate strain of CFRP sheet of 28 %, 34 %, and 41 % for 400 mm, 600 mm, and 800 mm, respectively. While, the percentage of beams exposed to 150ºC with a percentage concerning the ultimate strain of CFRP sheet of 26 %, 32 %, and 38 % for 400 mm, 600 mm, and 800 mm, respectively, and this equivalent to 0.93 of the beams strains exposed to 23 °C. The percentage of beams exposed to 250 °C with a percentage for the ultimate strain of CFRP sheet of 23 %, 26 %, and 31 % for 400 mm, 600 mm, and 800 mm, respectively, and this equivalent to 0.76 of the beams strains exposed to 23 °C. Finally, the percentage of beams exposed to 500 °C with a percentage for the ultimate strain of the CFRP sheet of 20 %, 32 %, 26 % for 400 mm, 600 mm, and 800 mm, respectively, and this equivalent to 0.63 of the beams strains exposed to 23 °C.

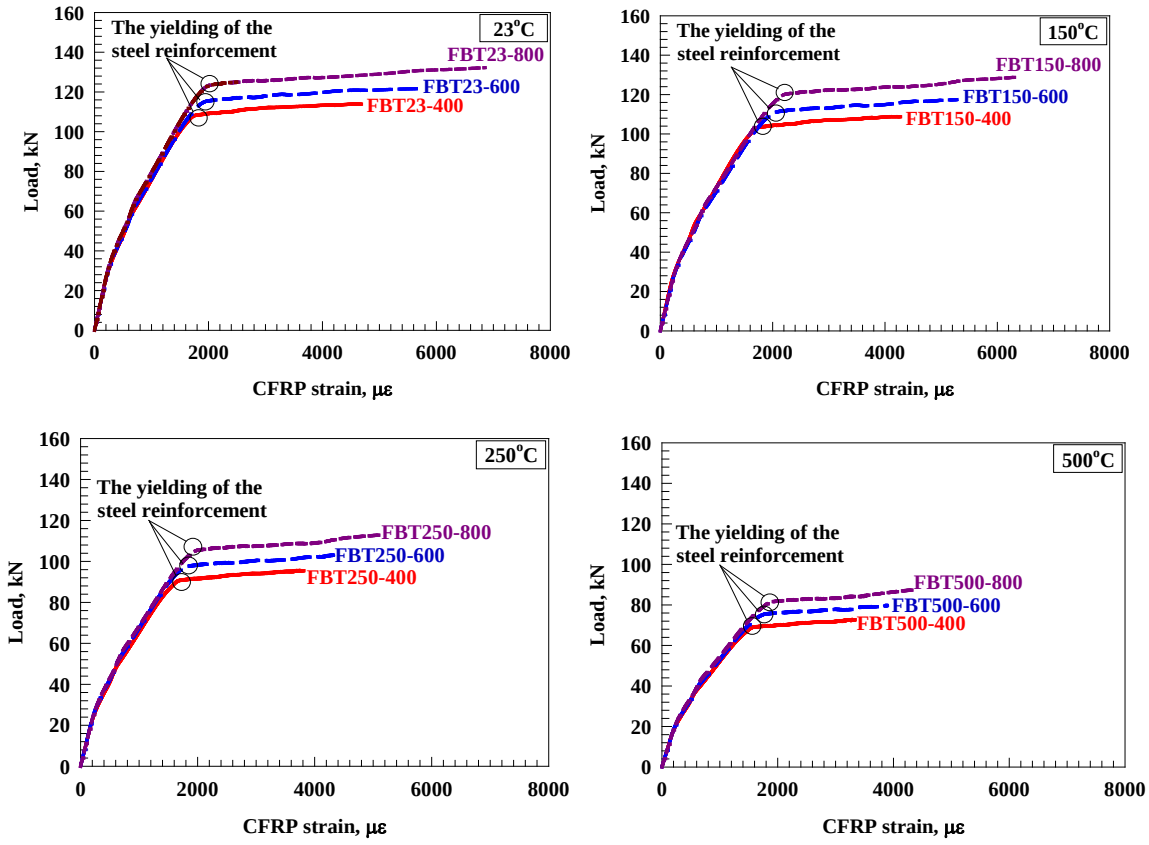

Figure 7. Typical load-CFRP strain curve.

CFRP strain development was less than 2000 με (12 % of the ultimate strain of CFRP sheet) before the steel reinforcement yielding. After the steel reinforcement yield, the CFRP strain increased rapidly and continued to increase until the beam failure, as shown in Fig. 7. It can be observed that the strain in the CFRP developed at a high rate as the applied load increases.

3.3. Load-deflection behavior

The load versus mid-span deflection curves for typically tested beams are shown in Fig. 8. The mid-span deflection curves are plotted in a way that allows for comparing the effect of CFRP sheet length for beams in terms of elevated temperature. Inspection of Fig. 8 reveals that the load-deflection curve can be divided into two stages; the first stage is from zero loadings up to yielding of steel reinforcement (Stabilization of the behavior) with nearly a straight line with rapidly increasing in load and slightly increasing in deflection. Then after the yielding of steel reinforcement (indicating a reduction in the beam stiffness and the CFRP sheets handled the applied load), the slope of the curve experienced a slight increase in the load with a large increase in deflection, and this is based on investigated parameters. At ultimate load, the load was dropped suddenly to zero after crashing of the compression zone. The load versus mid-span deflection curves for control and damaged beams showed similar trend behavior, as depicted in Fig. 8: curves were linear up to a certain point before became nonlinear. A limited linear portion can be clearly noticed for damaged beams because of concrete's thermal cracking. Similar trend behavior was noticed by Haddad and Almomani [33] in which the curves showed linear behavior at the initial stages of loading before turned nonlinear behavior thereafter. The degradation in mechanical properties and softening in damaged beams is referred to as the reduction in (a) the yield strength of steel reinforcing bars; (b) bond strength between steel reinforcement and concrete; and (c) concrete compressive strength, which was reduced by about 61 % of its intact value. Inspection of Fig. 8 reveals that the load-deflection curve was extensively affected by elevated temperature and CFRP bonded length in terms of ultimate load, ultimate deflection, toughness, and stiffness reflected either limited improvement and even degradation in the mechanical response of strengthened damaged, as compared to un-damaged control beams, as depicted in Fig. 8. In addition, the larger CFRP bonded length showed better performance than those with a small CFRP bonded length. Besides, the curve's performance decreased with the increase of exposed temperature, as shown in Fig. 8.

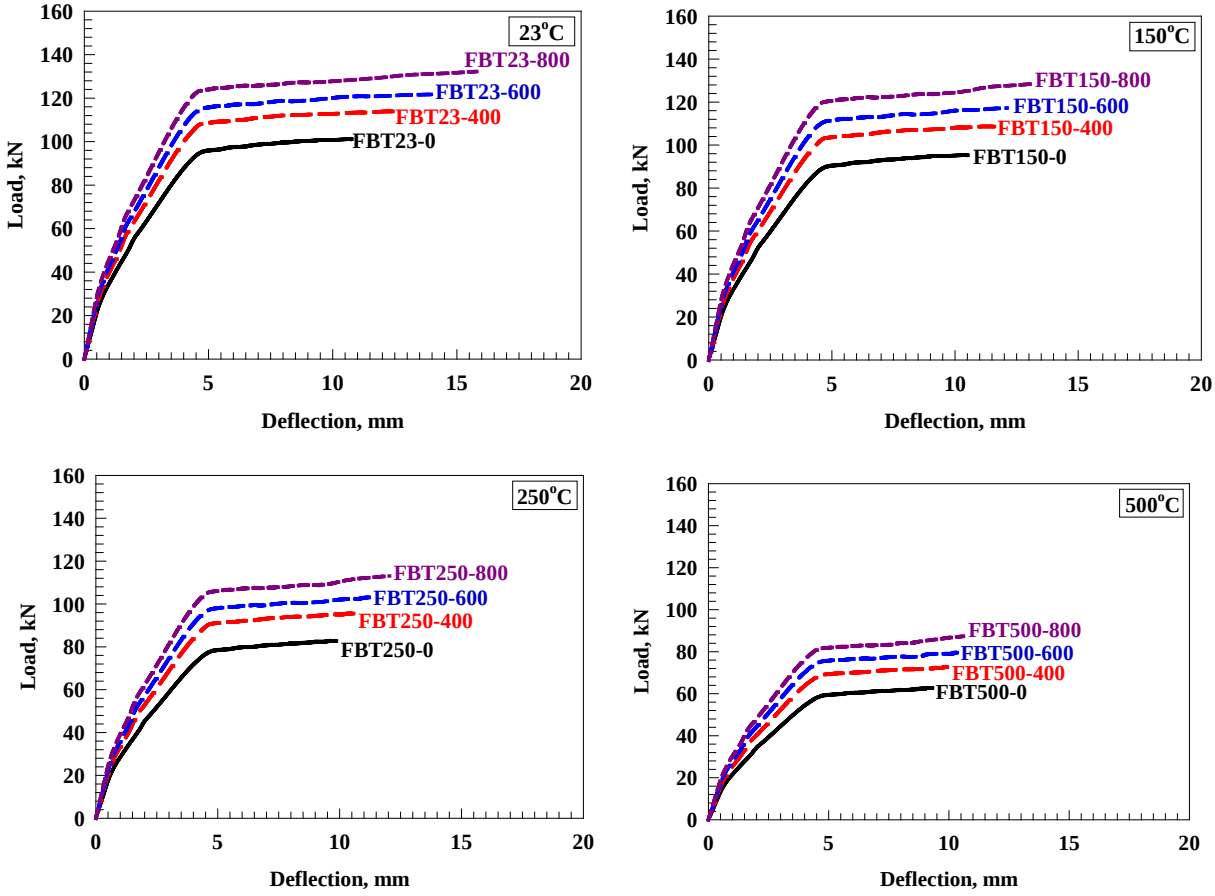

Figure 8. Load-deflection curves for the tested beam.

3.4. Ultimate load capacity and corresponding deflection

Table 3 shows the characteristics of the load-deflection curves for tested beams. The assessment of beams for load capacity and corresponding deflection shows the excellent performance of RC members. For strengthened RC members, deflection and ultimate load capacity can be related to the serviceability, and ultimate load limit states, respectively, as shown in Table 3. The load capacity and deflection percentages are defined as the ultimate load capacity and deflection, respectively, of CFRP strengthened beam divided by the ultimate deflection and load capacity of the un-strengthened beam (undamaged beam) as shown in Fig. 9. The strength ratio also predicts the increase of load that the model can sustain. Inspection of Fig. 9 reveals that the strength percentage increased significantly with the increase of the length of CFRP sheets. The average ultimate load enhancement percentage (Fig. 9) for tested beams with respect to the control beam is 14 %, 24 %, and 35 % for 400 mm, 600 mm, and 800 mm, respectively. Whereas, the average ultimate load reduction percentage (Fig. 9) for tested beams with respect to beams exposed to 23 °C is 4 %, 16 %, and 36 % for 150 °C, 250 °C, and 500 °C, respectively. Thus, it is possible to regain the 96 %, 84 %, and 64 % of the initial capacity of un-damaged beam (23 °C) 150 °C, 250 °C, and 500 °C, respectively. Therefore, the regaining percentage of the initial capacity is decreased with the increase of exposed temperature.

Table 3. Characteristics of load-deflection behavior.

Group	Specimen	T, °C	Elastic stiffness (kN/mm)	Toughness (kN.mm^2)	SF	DF	PF
1	FBT23-0	23	29.0	871	2.26	1.06	2.40
	FBT23-400		34.6	1187	2.69	1.26	3.40
	FBT23-600		37.3	1438	2.99	1.50	4.48
	FBT23-800		40.3	1783	3.43	1.79	6.12
2	FBT150-0	150	27.4	799	2.21	1.04	2.30
	FBT150-400		33.1	1033	2.49	1.23	3.08
	FBT150-600		35.9	1172	2.59	1.47	3.80
	FBT150-800		39.3	1413	2.87	1.75	5.02
3	FBT250-0	250	23.7	640	2.08	0.97	2.02
	FBT250-400		29.0	818	2.29	1.16	2.65
	FBT250-600		31.6	938	2.40	1.38	3.31
	FBT250-800		34.5	1109	2.61	1.64	4.28
4	FBT500-0	500	18.0	451	1.96	0.92	1.80
	FBT500-400		22.1	570	2.14	1.09	2.33
	FBT500-600		24.4	657	2.22	1.30	2.88
	FBT500-800		26.6	734	2.30	1.55	3.56

Note: SF: strength factor, DF: Ductility factor, PF: Performance Factor = SFxDF

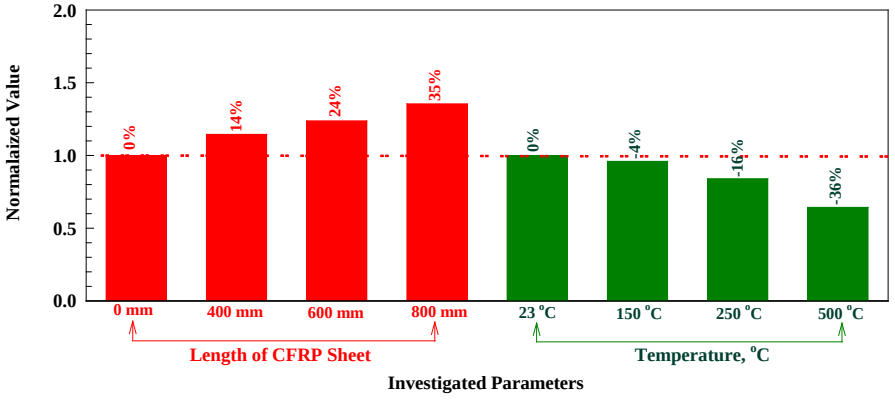

Figure 9. Normalized ultimate load capacity for control beam.

The deflection indicates how much the strengthened RC beams can sustain deformations without failure. The deflection percentage is defined as the ratio of the strengthened beam's ultimate deflection to the ultimate deflection of the control beam (undamaged beam), as shown in Fig. 10. Fig. 10 shows that the ductility percentage also significantly increased with the increase in the length of CFRP sheets and decreased with exposed temperature. The average ultimate deflection enhancement percentage (Fig. 10) for tested beams with respect to control beam is of 10 %, 18 %, and 27 % for 400 mm, 600 mm, and 800 mm, respectively, and this equal to 0.71 times the enhancement percentages in ultimate load. Whereas, the average ultimate deflection reduction percentage (Fig. 10) for tested beams with respect to beams exposed to 23 °C is 10 %, 17 %, and 23 % for 150 °C, 250 °C, and 500 °C strips, respectively, and this equal to 0.64 times the reduction percentages in ultimate load.

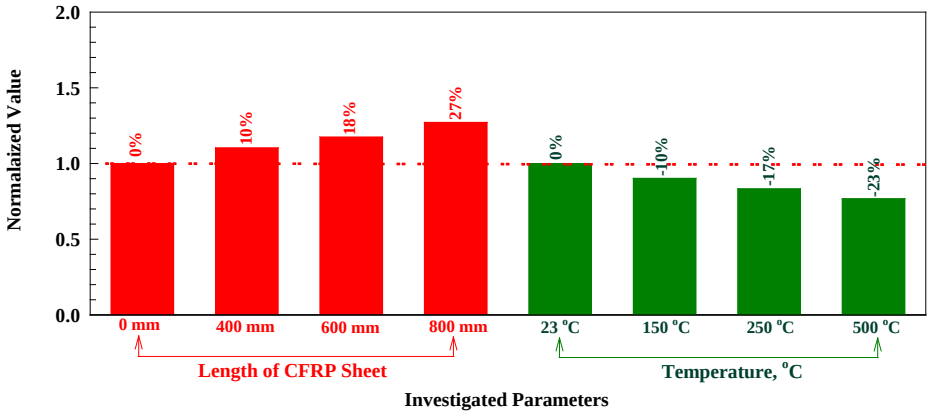

Figure 10. Normalized ultimate deflection for control beam.

3.5. Elastic stiffness

The elastic stiffness determines the crystal's response to an externally applied strain (or stress) and provides information about the bonding characteristics, mechanical and structural stability. The elastic stiffness represents the first stage of the load-deflection curve's slope before initiation of the first main flexural crack. For comparison, each strengthened beam's elastic stiffness with CFRP sheets was normalized for the control beam without CFRP sheets, as shown in Fig. 11. Fig. 11 reveals that the elastic stiffness percentage increased significantly with the increase of length of CFRP sheets. The average elastic stiffness enhancement percentage (Fig. 11) for tested beams with respect to control beam is of 21 %, 32 %, and 44 % for 400 mm, 600 mm, and 800 mm, respectively. Whereas, the average elastic stiffness reduction percentage (Fig. 11) for tested beams with respect to beams exposed to 23 °C is 7 %, 15 %, and 37 % for 150 °C, 250 °C, and 500 °C strips, respectively.

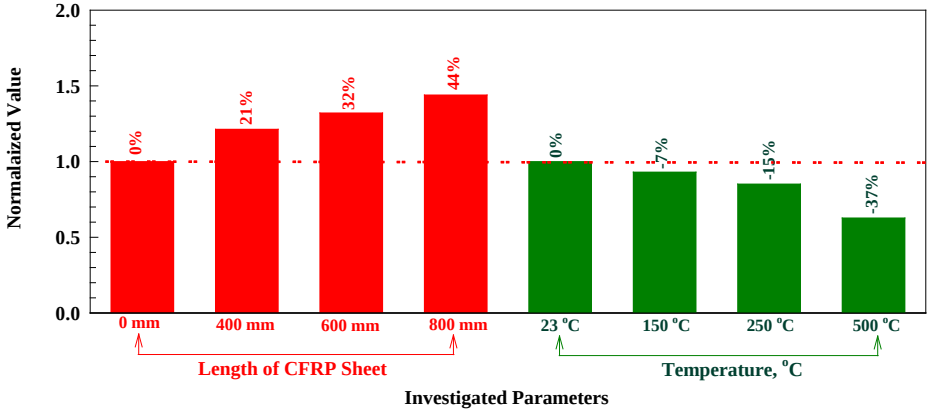

Figure 11. Normalized stiffness for control beam.

3.6. Toughness

In materials science and metallurgy, toughness is the ability to absorb energy and plastically deform without fracturing. One definition of material toughness is the amount of energy per unit volume that a material can absorb before rupturing. Toughness is calculated as the entire area under the load-deflection curve. In addition, the toughness of each strengthened beam with CFRP sheets was normalized with respect to the control beams without CFRP sheets as shown in Fig. 12. Inspection of Fig. 12 reveals that the toughness percentage increased significantly with the increase of length of CFRP sheets. The average toughness enhancement percentage (Fig. 12) for tested beams with respect to control beam is of 30 %,

51 %, and 79 % for 400 mm, 600 mm, and 800 mm, respectively. Whereas, the average toughness reduction percentage (Fig. 12) for tested beams with respect to beams exposed to 23 °C is 15 %, 33 %, and 53 % for 150 °C, 250 °C, and 500 °C strips, respectively.

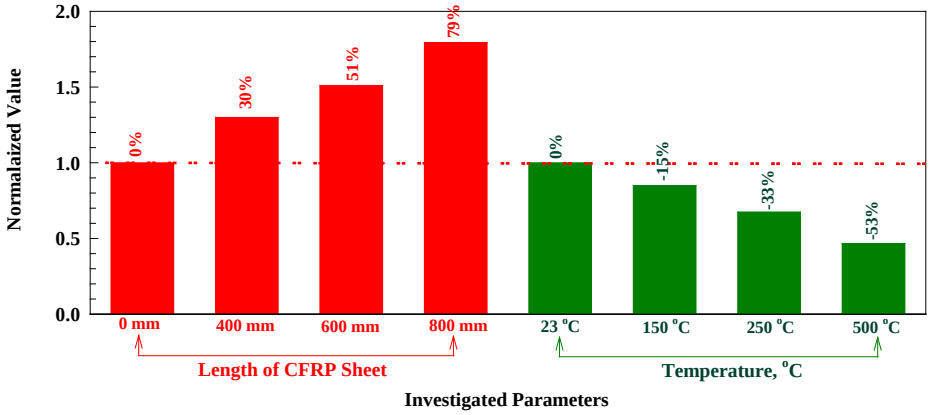

Figure 12. Normalized toughness with respect to control beam.

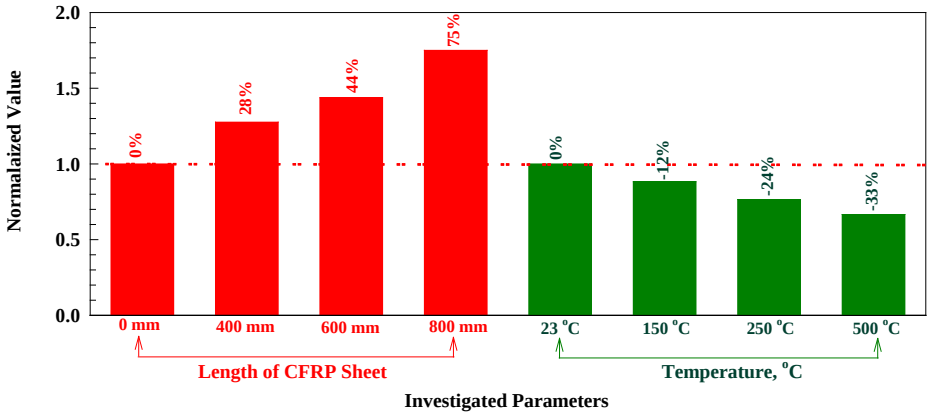

Figure 13. Normalized performance factor for control beam.

3.7. Evaluation of Performance of Experimental Results

The terms deformability factor (DF) and strength factor (SF) can then be defined as the deflection and the ultimate load capacity, respectively, of the strengthened beam, compared with the control beam. The strengthened composite beam's overall structural performance can thus be evaluated by a performance factor (PF), defined as DF multiplied by SF. Performance factor is a combination of the strength factor and the deformability factor to generate an overall structural performance as shown in Table 3 and Fig. 13. Based on Fig. 13 the PF increased as the length of CFRP sheets (bonded area of CFRP) increased and decreased with elevated temperature. Inspection of Fig. 13 reveals that the performance factor percentage increased significantly with the increase of the length of CFRP sheets. The average performance factor enhancement percentage (Fig. 12) for tested beams with respect to the control beam is 28 %, 44 %, and 75 % for 400 mm, 600 mm, and 800 mm, respectively. The average performance factor reduction percentage (Fig. 12) for tested beams for beams exposed to 23 °C is 12 %, 24 %, and 33 % for 150 °C, 250 °C, and 500 °C strips, respectively.

3.8. Comparison of experimental results with the ACI model

For comparison, the experimental results are compared with the ACI model [30]. The general design guidance is derived from the experimental data and is only applicable to external FRP reinforcement. Fig. 14 shows a comparison of the results predicted by the ACI model (Pf, experimental /Pf,ACI [30]). Note that the ACI model was calibrated for CFRP should be used with caution for other types of composites, as shown in Fig. 14. The overall predictions by ACI model [30] appear to be overestimated for beams strengthened with 400 mm, 600 mm, and 800 mm with a mean Pf, experimental /Pf,ACI value of 1.02, 1.06 and 1.09, respectively, and a coefficient of variation (COV) of 13 %. It is also important to consider that all the ACI model are semi-empirical, with important governing parameters derived from test data for beams strengthened with FRP sheets. In contrast, the ACI model cannot be applied in certain cases. Also, a careful inspection of Fig. 14 will show that the ACI model [30] has a much more comprehensive range of experimental/theoretical failure load ratios of 1.02 to 1.09.

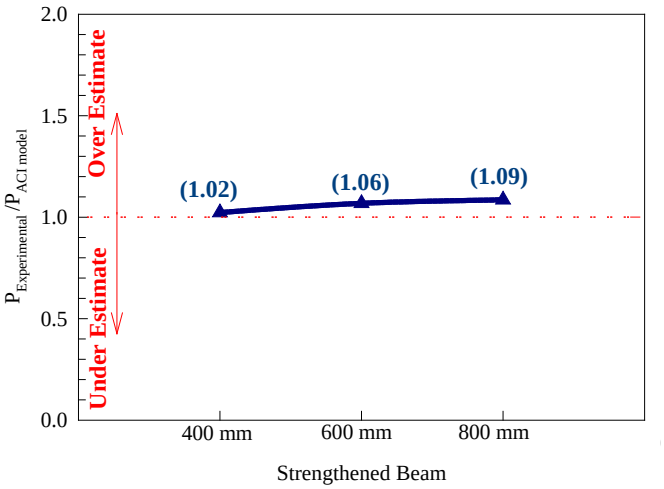

Figure 14. The normalized *e*xperimental FRP flexural force with respect to ACI model [30].

4. Conclusions

1. The CFRP sheet bridged the flexural cracks by providing adequate development length in catching the two sides of the major flexural crack.

2. The load-deflection curve can be divided into two stages; the first portion is nearly a straight line and the second stage with slope experienced a slight increase in the load with a large increase in deflection. The second stage is formed after steel reinforcement and the primary flexural crack formation, where the CFRP sheet carries the applied load.

3. The influence of the number of CFRP strips on the ductility, energy absorption, and ultimate load improvement percentage is significant.

4. The influence of the exposed temperature on the ductility, energy absorption, and ultimate load reduction percentage is significant and increased with the increase of temperature.

5. It is encouraging advantage of using the CFRP sheets along the bottom face of the beam to enhance the beam integrity before and after cracking (ductile failure mode), external arresting the flexural cracks, and improving the structural performance and serviceability of tested beam.

6. The ACI model [30] appears to be overestimated with a coefficient of variation (COV) of 13 %.

5. Acknowledgment

The author gratefully acknowledges the financial support from Deanship of Scientific Research at Jordan University of Science and Technology under Grant number 2019/507.

References

1. Al-Rousan, R.Z. Empirical and NLFEA prediction of bond-slip behavior between DSSF concrete and anchored CFRP composites. Construction and Building Materials. 2018. 169(1). Pp. 530–542. DOI: 10.1016/j.conbuildmat.2018.03.013
2. Al-Rousan, R.Z. Behavior of macro synthetic fiber concrete beams strengthened with different CFRP composite configurations. Journal of Building Engineering. 2018. 20(1). Pp. 595–608. DOI: 10.1016/j.jobe.2018.09.009
3. Al-Rousan, R.Z. Isra'a, A.-M. Bending and Torsion Behaviour of CFRP Strengthened RC Beams. Magazine of Civil Engineering. 2019. 92(8). Pp. 62–71. DOI: 10.18720/MCE.92.8
4. Travush, V.I., Konin, D.V., Krylov, A.S. Strength of reinforced concrete beams of high-performance concrete and fiber reinforced concrete. Magazine of Civil Engineering. 2018. 77(1). Pp. 90–100. DOI: 10.18720/MCE.77.8
5. Kodur, V., Agrawal, A. An approach for evaluating residual capacity of reinforced concrete beams exposed to fire. Engineering Structures. 2016. 110(1). Pp. 293–306. DOI: 10.1016/j.engstruct.2015.11.047
6. Al-Ostaz, A.M., Irshidat, B., Tenkhoff, P.S. Ponnapalli. Deterioration of bond integrity between repair material and concrete due to thermal and mechanical incompatibilities. Journal of Materials in Civil Engineering. 2010. 22(2). Pp. 136–144. DOI: 10.1061/(ASCE)0899-1561(2010) 22:2(136)
7. Nedviga, E., Beresneva, N., Gravit, M., Blagodatskaya, A. Fire Resistance of Prefabricated Monolithic Reinforced Concrete Slabs of "Marko" Technology. Adv. Intell. Syst. Comput. 2018. 692(1). Pp. 739–749. DOI: 10.1007/978-3-319-70987-1_78
8. Hezhev, T.A., Zhurtov, A.V., Tsipinov, A.S., Klyuev, S.V. Fire resistant fibre reinforced vermiculite concrete with volcanic application. Magazine of Civil Engineering. 2018. 80(1). Pp. 181–194. DOI: 10.18720/MCE.80.16
9. Goremikins, V., Blesak, L., Novak, J., Wald, F. Experimental investigation on SFRC behaviour under elevated temperature. Journal of Structural Fire Engineering. 2017. 8(1). Pp. 287–299. DOI: 10.1108/JSFE-05-2017-0034

10. Goremikins, V., Blesak, L., Novak, J., Wald, F. To testing of steel fibre reinforced concrete at elevated temperature. Applications of Structural Fire Engineering. 2017. 1(1). Pp. 48–54. DOI: 10.14311/asfe.2015.055
11. Blesak, L., Goremikins, V., Wald, F., Sajdlova, T. Constitutive model of steel fibre reinforced concrete subjected to high temperatures. Acta Polytechnica. 2016. 56(1). Pp. 417–424. DOI: 10.14311/AP.2016.56.0417
12. Korsun, V., Vatin, N., Franchi, A., Korsun, A., Crespi, P., Mashtaler, S. The strength and strain of high-strength concrete elements with confinement and steel fiber reinforcement including the conditions of the effect of elevated temperatures. Procedia Engineering. 2015. 117(1). Pp. 970–979. DOI: 10.1016/j.proeng.2015.08.192
13. Goremikins, V., Blesak, L., Novak, J., Wald, F. Experimental method on investigation of fibre reinforced concrete at elevated temperatures. Acta Polytechnica. 2016. 56(1). Pp. 258–264. DOI: 10.14311/AP.2016.56.0258
14. Selyaev, V.P., Nizina, T.A., Balykov, A.S., Nizin, D.R., Balbalin, A.V. Fractal analysis of deformation curves of fiber-reinforced fine-grained concretes under compression. PNRPU Mechanics Bulletin. 2016. 1(1). Pp. 129–146. DOI: 10.15593/perm.mech/2016.1.09
15. Bily, P., Fladr, J., Kohoutkova, A. Finite Element Modelling of a Prestressed Concrete Containment with a Steel Liner. Proceedings of the Fifteenth International Conference on Civil, Structural and Environmental Engineering Computing. Civil-Comp Press. 2015. DOI: 10.4203/ccp.108.1
16. Bílý, P., Kohoutková, A. Sensitivity analysis of numerical model of prestressed concrete containment. Nuclear Engineering and Design. 2015. 295(1). Pp. 204–214. DOI: 10.1016/j.nucengdes.2015.09.027
17. Al-Rousan, R. Behavior of two-way slabs subjected to drop-weight. Magazine of Civil Engineering. 2019. 90(6). Pp. 62–71. DOI: 10.18720/MCE.90.6
18. Al-Rousan, R. The impact of cable spacing on the behavior of cable-stayed bridges. Magazine of Civil Engineering. 2019. 91(7). Pp. 49–59. DOI: 10.18720/MCE.91.5
19. Krishan, A., Rimshin, V., Erofeev, V., Kurbatov, V., Markov, S. The energy integrity resistance to the destruction of the long-term strength concrete. Procedia Engineering. 2015. 117(1). Pp. 211–217. DOI: 10.1016/j.proeng.2015.08.143
20. Korsun, V., Vatin, N., Korsun, A., Nemova, D. Physical-mechanical properties of the modified fine-grained concrete subjected to thermal effects up to 200°S. Applied Mechanics and Materials. 2014. 633–634. Pp. 1013–1017. DOI: 10.4028/www.scientific.net/AMM.633-634.1013
21. Korsun, V., Korsun, A., Volkov, A. Characteristics of mechanical and rheological properties of concrete under heating conditions up to 200°C. MATEC Web Conference. 2013. 6(1). Pp. 07002. DOI: 10.1051/matecconf/20130607002
22. Petkova, D., Donchev, T., Wen, J. Experimental study of the performance of CFRP strengthened small scale beams after heating to high temperatures. Construction and Building Materials. 2014. 68(1). Pp. 55–61. DOI: 10.1016/j.conbuild-mat.2014.06.014
23. Ji, G., Li, G., Alaywan, W. A new fire resistant FRP for externally bonded concrete repair. Construction and Building Materials. 2013. 42(1). Pp. 87–96. DOI: 10.1016/j.conbuildmat.2013.01.008
24. Trentin, C., Casas, J.R. Safety factors for CFRP strengthening in bending of reinforced concrete bridges. Composite Structures. 2015. 128(1). Pp. 188–198. DOI: 10.1016/j.compstruct.2015.03.048
25. Ferrari, V.J., Hanai, J.B. de, Souza, R.A. de. Flexural strengthening of reinforcement concrete beams using high performance fiber reinforcement cement-based composite (HPFRCC) and carbon fiber reinforced polymers (CFRP). Construction and Building Materials. 2013. 48(1). Pp. 485–498. DOI: 10.1016/j.conbuildmat.2013.07.026
26. Attari, N., Amziane, S., Chemrouk, M. Flexural strengthening of concrete beams using CFRP, GFRP and hybrid FRP sheets. Construction and Building Materials. 2012. 37(1). Pp. 746–757. DOI: 10.1016/j.conbuildmat.2012.07.052
27. Rami, H. Haddad, Rajai Al-Rousan, Ashraf Almasry. Bond-slip behavior between carbon fiber reinforced polymer sheets and heat-damaged concrete. Composites Part B: Engineering. 2013. 45(1). Pp. 1049–1060. DOI: 0.1016/j.compositesb.20-12.09.010
28. Kara, I.F., Ashour, A.F., Körog˘lu, M.A. Flexural behavior of hybrid FRP/steel reinforced concrete beams. Composite Structures. 2015. 129(1). Pp. 111–121. DOI: 10.1016/j.compstruct.2015.03.073
29. Kolchunov, V.I., Dem'yanov, A.I. The modeling method of discrete cracks in reinforced concrete under the torsion with bending. Magazine of Civil Engineering. 2018. 81(5). Pp. 160–173. DOI: 10.18720/MCE.81.16
30. ACI Committee 440. Design and Construction of Externally Bonded FRP Systems for strengthening Concrete Structures. *ACI440.2R-02. 2002. American Concrete Institute, Farmington Hills, Mich.: 45 p. DOI: 10.1061/40753(171)159. ISBN: 9780-870312854
31. Roberto Pagani, Massimiliano Bocciarelli, Valter Carvelli, Marco Andrea Pisani. Modelling high temperature effects on bridge slabs reinforced with GFRP rebars. Engineering Structures. 2014. 81(1). Pp. 318–326. DOI: 10.1016/j.engstruct.2014.10.012
32. Ahmed Hassan, Faisal Aldhafairi, L.M., Abd-EL-Hafez, A.E.Y. Abouelezz. Retrofitting of different types of reinforced concrete beams after exposed to elevated temperature. Engineering Structures. 2019. 194(1). Pp. 420-430. DOI: 10.1016/j.engstruct.2019.05.084
33. Haddad Rami, H., Almomani Oubaida, A. Recovering flexural performance of thermally damaged concrete beams using NSM CFRP strips. Construction and Building Materials. 2017. 154(1). Pp. 632–643. DOI: 10.1016/j.conbuildmat.2017.07.211

Contacts:

Rajai Al-Rousan, rzalrousan@just.edu.jo